NEURONAL MODELING

Single-trial spike trains in parietal cortex reveal discrete steps during decision-making

Kenneth W. Latimer,[1,2] Jacob L. Yates,[1,2] Miriam L. R. Meister,[2,3] Alexander C. Huk,[1,2,4,5] Jonathan W. Pillow[1,2,5,6]*

Neurons in the macaque lateral intraparietal (LIP) area exhibit firing rates that appear to ramp upward or downward during decision-making. These ramps are commonly assumed to reflect the gradual accumulation of evidence toward a decision threshold. However, the ramping in trial-averaged responses could instead arise from instantaneous jumps at different times on different trials. We examined single-trial responses in LIP using statistical methods for fitting and comparing latent dynamical spike-train models. We compared models with latent spike rates governed by either continuous diffusion-to-bound dynamics or discrete "stepping" dynamics. Roughly three-quarters of the choice-selective neurons we recorded were better described by the stepping model. Moreover, the inferred steps carried more information about the animal's choice than spike counts.

Ramping responses have been observed in a variety of brain areas during decision-making and have been widely interpreted as the neural implementation of evidence accumulation for forming decisions (*1*–*7*). However, ramping can only be observed by averaging together responses from many trials (and, often, many neurons), which obscures the dynamics governing responses on single trials. In particular, a discrete "stepping" process (*8*, *9*), in which the spike rate jumps stochastically from one rate to another at some time during each trial, can also create the appearance of ramping (*10*, *11*). Although decision-making at the behavioral level is well described as an accumulation process (*12*, *13*), whether the brain computes decisions through a direct neural correlate (ramping) or a discrete implementation (stepping) remains a central, unresolved question in systems neuroscience.

We used advanced statistical methods to identify the single-trial dynamics governing spike trains in the lateral intraparietal (LIP) area of macaques performing a well-studied motion-discrimination task (Fig. 1A) (*3*, *14*). We formulated two spike-train models with stochastic latent dynamics governing the spike rate: one defined by continuous ramping dynamics and the other by discrete stepping dynamics (see the supplementary methods for mathematical details). In the ramping model, also known as "diffusion-to-bound," the spike rate evolves according to a Gaussian random walk with linear drift (Fig. 1B). The slope of drift depends on the strength of sensory evidence, and each trial's trajectory continues until hitting an absorbing upper bound. Alternatively, in the stepping model, the latent spike rate jumps instantaneously from an initial "undecided" state to one of two discrete decision states during the trial (Fig. 1C). The probability of stepping up or stepping down and the timing of the step are determined by the strength of sensory evidence. For both models, we assumed that spiking follows an inhomogeneous Poisson process given the time-varying spike rate.

Both latent variable models are "doubly stochastic" in the sense that the probability of an observed spike train given the sensory stimulus depends on both the noisy trajectory of the latent spike rate and the Poisson variability in the spiking process. Fitting such latent variable models requires integrating over all latent trajectories consistent with the observed spike trains, which is not analytically tractable. We therefore

[1]Center for Perceptual Systems, The University of Texas at Austin, Austin, TX 78712, USA. [2]Institute for Neuroscience, The University of Texas at Austin, Austin, TX 78712, USA. [3]Department of Physiology and Biophysics, University of Washington, Seattle, WA 98195, USA. [4]Department of Neuroscience, The University of Texas at Austin, Austin, TX 78712, USA. [5]Department of Psychology, The University of Texas at Austin, Austin, TX 78712, USA. [6]Princeton Neuroscience Institute and Department of Psychology, Princeton University, Princeton, NJ 08544, USA.
*Corresponding author. E-mail: pillow@princeton.edu

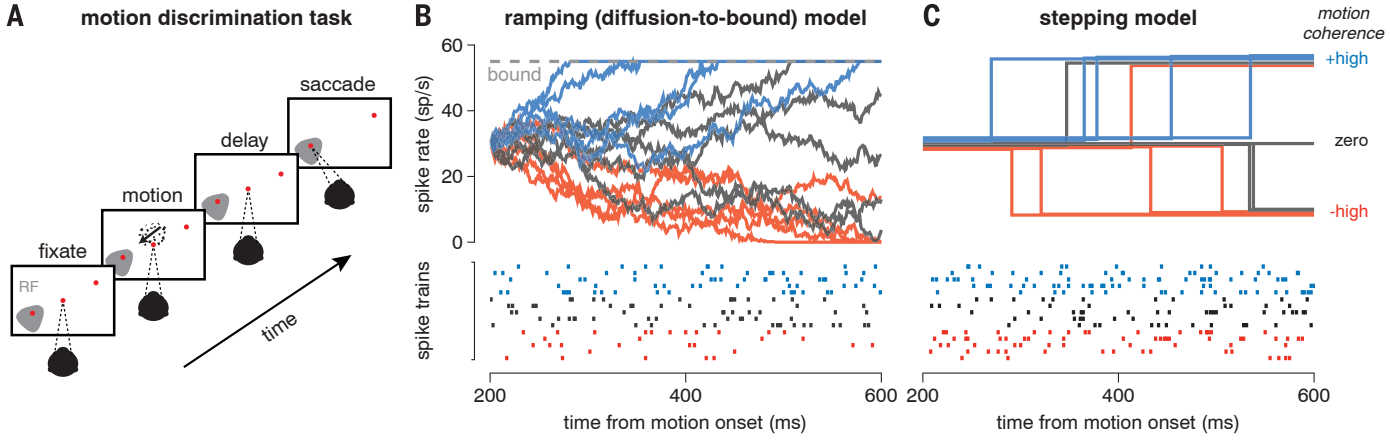

Fig. 1. Motion discrimination task and spike-train models. (**A**) Schematic of moving-dot direction-discrimination task. The monkey views and discriminates the net direction of a motion stimulus of variable motion strength and duration and indicates its choice by making a saccade to one of two choice targets 500 ms after motion offset. One choice target is in the response field of the neuron under study (RF, shaded patch on left); the other is outside it. (**B**) Ramping (diffusion-to-bound) model. Spike rate trajectories (solid traces) were sampled from a diffusion-to-bound process for each of three motion coherences (strong positive, zero, and strong negative). The model parameters include an initial spike rate, a slope for each coherence, noise variance, and an upper bound. We do not include a lower bound, consistent with the competing integrator (race) model of LIP (*5*). Spike trains (below) obey an inhomogeneous Poisson process for each spike rate trajectory. (**C**) Discrete stepping model. Spike rate trajectories (above) begin at an initial rate and jump up or down at a random time during each trial, and spike trains (below) once again follow a Poisson process, given the latent rate. The step times take a negative binomial distribution, which resembles the time-to-bound distribution under a diffusion model. Parameters include the spike rates for the three discrete states and two parameters governing the distribution over step timing and direction for each motion coherence. Both models were fit using the spike trains and coherences for each neuron, without access to the animal's choices.

developed sampling-based Markov chain Monte Carlo methods, which provide samples from the posterior distribution over model parameters and allow us to perform Bayesian model comparison.

We focused on a population of 40 neurons with highly choice-selective responses that exhibited ramping in their average responses (*14*), typically increasing during trials in which the monkey eventually chose the target inside the response field (RF) of the neuron and decreasing when the monkey chose the target outside the RF. We fit each neuron with both ramping and stepping models, using the spike-train data from 200 ms after motion onset (*15*) until 200 ms after motion offset (300 ms before the monkey received the "go" signal). Figure 2A shows the raster of spike trains from an example LIP neuron plotted in two different ways: first, aligned to the time of motion stimulus onset (left); and second, aligned to the step time inferred under the stepping model (right). The traditional raster and peristimulus time histogram (PSTH) at left show that the average response ramps upward or downward depending on choice, as expected. The step-aligned raster at right, however, shows that these data are also consistent with discrete steplike transitions with variable timing across trials. Additional panels show the distribution of step times inferred under the model (Fig. 2B), and the dependence of step direction (up or down) on the motion signal (Fig. 2C). Discrete steps in the instantaneous spike rate could thus plausibly underlie the gradual ramping activity seen in stimulus-aligned and averaged LIP spike responses.

We applied the same analysis to the full set of LIP neurons and observed similar structure in step-aligned rasters (figs. S13 to S15). Figure 3A shows population-averaged PSTHs computed from stimulus-aligned (left) and step-aligned responses, sorted by motion strength (middle), or motion strength and step direction (right). The middle and right plots show that spike rate is effectively constant when spike trains are aligned to the inferred step time on each trial. The multiple step heights observed in the middle plot result from the fact that the proportion of up and down steps varies with motion strength. The right plot confirms that the firing rate, once conditioned on stepping up or down, is

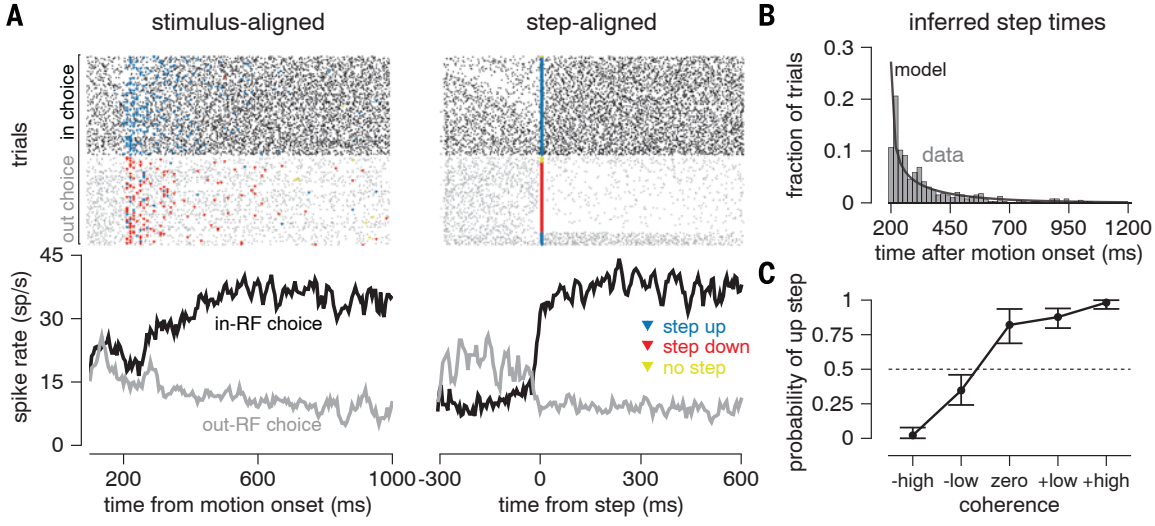

Fig. 2. Model-based analysis of spike responses from an example LIP neuron. (**A**) Spike rasters sorted by the monkey's choice in or out of the RF of the neuron under study (black, in-RF; gray, out-RF) and their associated averages (PSTHs, below). (Left) Conventional stimulus-aligned rasters with each trial aligned to the time of motion onset exhibit commonly observed ramping in the PSTH. Blue and red triangles indicate the inferred time of an up or down step on each trial under the fitted stepping model. Yellow triangles indicate that no step was found during the trial and are placed at the end of the trial segment we analyzed (200 ms after motion offset). (Right) The same spike trains aligned to the inferred step time for each trial. The estimated step direction of the neuron does not always match the animal's decision on each trial. (**B**) The distribution of inferred step times shown in (A) (histogram) and the distribution over step times under the fitted parameters (black trace). (**C**) The probability of an up step for each coherence level. Error bars, 95% CIs.

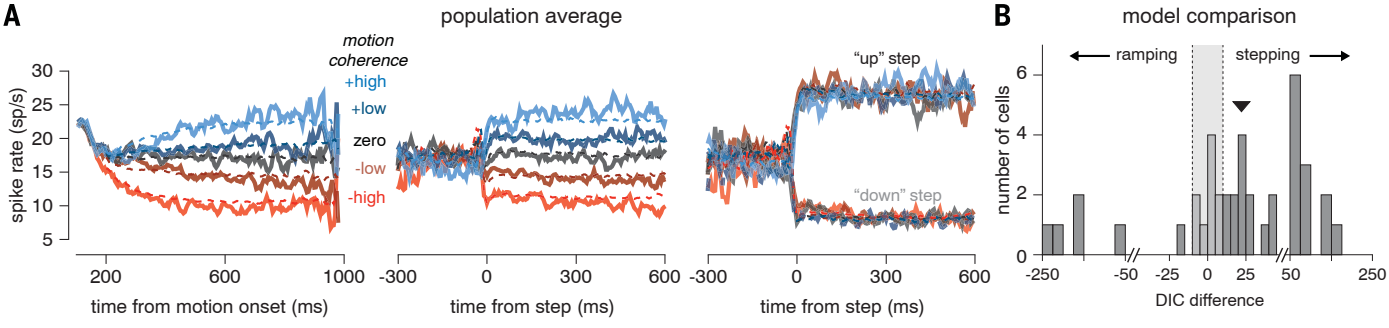

Fig. 3. Stepping model captures LIP responses. (**A**) Population average PSTH sorted by motion coherence computed from spike trains: (Left) Aligned to motion onset and sorted by motion strength. (Middle) Aligned to step times inferred under the stepping model and sorted by motion strength. (Right) Aligned to step times and sorted by both motion strength and inferred step direction. Simulated results from the stepping model (dashed lines) provide a close match to the real data under all types of alignment and conditioning. (**B**) Quantitative model comparison using DIC reveals a superior fit of the stepping model over the ramping model for the majority of cells (31 out of 40). A DIC difference greater than ±10 (gray region) is commonly regarded as providing strong support for one model over the other (*22*). We found substantially more cells with strong evidence for stepping over ramping (25 cells versus 6 cells; median DIC difference = 22.1; sign test $P < 0.001$).

independent of motion strength. Furthermore, simulated spike responses, based on the fitted stepping models, resemble the real data under both kinds of alignment (dashed traces).

Although these analyses provide a visually compelling illustration of the plausibility of stepping dynamics in LIP, they do not by themselves definitively rule out the ramping model (see fig. S16). Using our latent variable models, we can formally address this issue using statistical model comparison. Both models give a probability distribution over spike trains, and the model that better represents the data should place more probability mass over the observed spike trains. We compared the model fits using the deviance information criterion (DIC) (*16*), which integrates over the entire posterior distribution of model parameters given the data, thereby taking into account the uncertainty in the model fit as well as the number of parameters in each model.

The stepping model provided a superior account of LIP responses for 78% (31 out of 40) of the cells compared to the ramping model (Fig. 3B). The stepping model therefore not only accounts for the ramplike activity observed in averaged LIP responses, but its qualitative ability to reveal step times is bolstered by quantitative superiority in accounting for the statistical structure of spike trains for a majority of LIP neurons. The superiority was supported not just by DIC but also by other model comparison metrics, such as Bayes factors (fig. S1).

We subsequently examined how well the two models account for the time-varying mean and the variance of neural responses. Figure 4A shows the comparison for the mean responses (top row) and variance (bottom row) for the data (left column), stepping model (middle column), and ramping model (right column). Although the models were fit to predict the spike responses on each trial, as opposed to these summary statistics, both models did an acceptable job of accounting for the mean response [fraction of variance in the PSTHs explained: stepping R^2 = 0.94, 95% credible interval (CI) (0.90, 0.94); ramping R^2 = 0.78, 95% CI (0.71, 0.79)]. This is consistent with the long-standing difficulty in distinguishing between these two mechanisms. However, the stepping model provided a more accurate fit to the variance of neural responses [stepping R^2 = 0.40, 95% CI (0.09, 0.45); ramping R^2 = −0.49, 95% CI (−0.86, −0.27)]. In particular, the stepping model captured the decreasing variance observed in trials with strong negative motion much better than the ramping model. (A similar result held for estimates of variance of the underlying spike rate; see fig. S21).

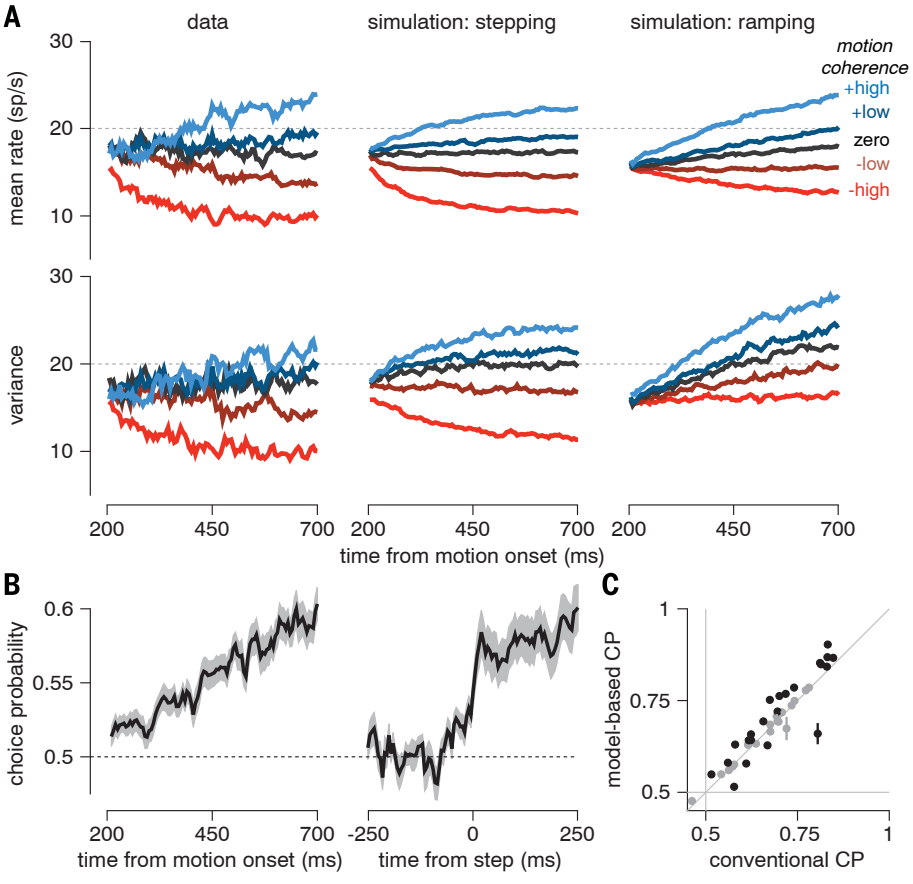

Fig. 4. Stepping model better explains variance of responses and can be used to decode choices. (**A**) Comparison of model fits to average population activity, sorted by stimulus strength. Motion coherence and direction are indicated by color (blue, in-RF; red, out-RF). Average spike rate (top) and spike count variance (bottom) for the population aligned to motion onset. The data (left) and simulations from the stepping model (center) and the diffusion-to-bound model (right) fits to all 40 cells are shown. Spike rates and variances were calculated with a 25-ms sliding window. (**B**) Population average CP aligned to stimulus onset (left) and average CP aligned to estimated step times (right). Gray region indicates mean ± 1 SEM. CPs were calculated with a sliding 25-ms window. Conventional alignment suggests a ramp in choice selectivity, and the model-based alignment indicates a rapid transition. (**C**) Conventional CP based on spike counts using responses 200 to 700 ms after motion onset versus model-based CP using the probability of stepping to the up state by the end of the same period. Model-based CP is greater than conventional CP in the population (Wilcoxon signed rank test; $P < 0.05$). Stepping models were fit using 10-fold cross-validation. Error bars show mean ± 1 SE of CPs, as computed on each training data set. Black points indicate cells with significant differences between model-based and conventional CP (Student's *t* test; $P < 0.05$), and gray indicates that differences were not significant.

Finally, the stepping model provides a platform for neural decoding, because the posterior distribution over the step can be used for reading out decisions from the spikes on a single trial. We first quantified decoding performance using choice probability (CP), a popular metric for quantifying the relationship between choice and spike counts. Aligned to motion onset, CP grows roughly linearly with time (Fig. 4B, left). However, the CP relative to the inferred step times (Fig. 4B, right) was consistent with an abrupt emergence of choice-related activity. We then compared classical CP with a model-based CP measure, which assumed that the direction of the neuron's step predicted the animal's choice. We reiterate that the model was fit to the spike trains without access to the animal's choices. The model-based CP was on average greater than classical CP, indicating that the states estimated under the stepping model were more informative about the animal's choice than raw spike counts (Fig. 4C).

In conclusion, we have developed tractable, principled methods for fitting and comparing statistical models of single-neuron spike trains in which spike rates are governed by a latent stochastic process. We have applied these methods to determine the dynamics underlying neural activity in area LIP. Although neurons in this area have been largely assumed to exhibit ramping dynamics, reflecting the temporal accumulation of evidence posited by models of decision-making, statistical model comparison supports an alternative hypothesis: LIP responses were better described by randomly timed, discrete steps between underlying states. [In a supplementary analysis, we examined data from a response-time version of the dots task and found results consistent with the fixed duration version; this initial comparison will be strengthened by extending the models to account for overlapping decision and motor events and application to larger data sets (figs. S23 to S25) (*17*)]. In addition to accounting better for the dynamics of the mean firing rates, only the stepping model accounts accurately for

the variance of neural responses. Finally, the estimation of single-trial step times provides a novel view of choice-related activity, revealing that choice-correlated fluctuations in response are also dominated by discrete steplike dynamics.

Although these results challenge the canonical perspective of LIP dynamics during decision-making, the approach facilitates new avenues of investigation. Our analyses suggest that accumulation may be implemented by stochastic steps, but simultaneous recordings of multiple neurons will be required to investigate whether population activity ramps or discretely transitions between states on single trials (*8*); population-level ramping could still be implemented via step times that vary across neurons, even on the same trial. Fortunately, the statistical techniques reported here are scalable to simultaneously recorded samples of multiple neurons, and newer recording techniques are starting to yield these multineuron data sets (*18*–*21*). It is also possible that single neurons with ramping dynamics implement evidence integration elsewhere in the brain and that LIP neurons are postdecisional or premotor indicators of the binary result of this computation. More generally, we believe that these techniques will have broad applicability for identifying and interpreting the latent factors governing multineuron spike responses, allowing for principled tests of the dynamics governing cognitive computations in many brain areas.

REFERENCES AND NOTES

1. M. E. Mazurek, J. D. Roitman, J. Ditterich, M. N. Shadlen, *Cereb. Cortex* **13**, 1257–1269 (2003).
2. J. I. Gold, M. N. Shadlen, *Annu. Rev. Neurosci.* **30**, 535–574 (2007).
3. R. Kiani, T. D. Hanks, M. N. Shadlen, *J. Neurosci.* **28**, 3017–3029 (2008).
4. R. Kiani, M. N. Shadlen, *Science* **324**, 759–764 (2009).
5. M. N. Shadlen, R. Kiani, *Neuron* **80**, 791–806 (2013).
6. M. N. Shadlen, W. T. Newsome, *Proc. Natl. Acad. of Sci.* **93**, 628–633 (1996).
7. T. D. Hanks *et al*., *Nature* **520**, 220–223 (2015).
8. P. Miller, D. B. Katz, *J. Neurosci.* **30**, 2559–2570 (2010).
9. D. Durstewitz, G. Deco, *Eur. J. Neurosci.* **27**, 217–227 (2008).
10. M. S. Goldman, *Encyclopedia of Computational Neuroscience*, D. Jaeger, R. Jung, Eds. (Springer, New York, 2015), pp. 1177–1182.
11. A. K. Churchland *et al*., *Neuron* **69**, 818–831 (2011).
12. R. Ratcliff, J. N. Rouder, *Psychol. Sci.* **9**, 347–356 (1998).
13. B. W. Brunton, M. M. Botvinick, C. D. Brody, *Science* **340**, 95–98 (2013).
14. M. L. R. Meister, J. A. Hennig, A. C. Huk, *J. Neurosci.* **33**, 2254–2267 (2013).
15. A. K. Churchland, R. Kiani, M. N. Shadlen, *Nat. Neurosci.* **11**, 693–702 (2008).
16. D. J. Spiegelhalter, N. G. Best, B. P. Carlin, A. van der Linde, *J. R. Stat. Soc. Series B Stat. Methodol.* **64**, 583–639 (2002).
17. J. D. Roitman, M. N. Shadlen, *J. Neurosci.* **22**, 9475–9489 (2002).
18. I. H. Stevenson, K. P. Kording, *Nat. Neurosci.* **14**, 139–142 (2011).
19. A. Bollimunta, D. Totten, J. Ditterich, *J. Neurosci.* **32**, 12684–12701 (2012).
20. R. Kiani, C. J. Cueva, J. B. Reppas, W. T. Newsome, *Curr. Biol.* **24**, 1542–1547 (2014).
21. M. T. Kaufman, M. M. Churchland, S. I. Ryu, K. V. Shenoy, *eLife* **4**, e04677 (2015).
22. K. P. Burnham, D. R. Anderson, *Model Selection and Multimodel Inference: A Practical Information-Theoretic Approach* (Springer Science & Business Media, New York, 2002).

ACKNOWLEDGMENTS

We thank I. Memming Park and C. Carvalho for constructive discussions and J. Roitman and M. Shadlen for public sharing of data. This research was supported by grants from the National Eye Institute (EY017366 to A.C.H.) and the National Institute of Mental Health (MH099611 to J.W.P. and A.C.H.), by the Sloan Foundation (J.W.P.), McKnight Foundation (J.W.P.), a National Science Foundation CAREER award (IIS-1150186 to J.W.P.), and the National Institutes of Health under Ruth L. Kirschstein National Research Service Awards T32DA018926 from the National Institute on Drug Abuse and T32EY021462 from the National Eye Institute. All behavioral and electrophysiological data are presented in (*14*) and are archived at the Center for Perceptual Systems, The University of Texas at Austin.

SUPPLEMENTARY MATERIALS

www.sciencemag.org/content/349/6244/184/suppl/DC1
Materials and Methods
Supplementary Text
Figs. S1 to S25
Tables S1 and S2
References (*23*–*33*)

1 December 2014; accepted 10 June 2015
10.1126/science.aaa4056

PROTEIN STRUCTURE

Crystal structure of a mycobacterial Insig homolog provides insight into how these sensors monitor sterol levels

Ruobing Ren,[1,2,3]* Xinhui Zhou,[1,2,3]* Yuan He,[1,2,3] Meng Ke,[1,2,3] Jianping Wu,[1,2,3] Xiaohui Liu,[4] Chuangye Yan,[1,2,3] Yixuan Wu,[1,2,3] Xin Gong,[1,2,3] Xiaoguang Lei,[4] S. Frank Yan,[5] Arun Radhakrishnan,[6] Nieng Yan[1,2,3]†

Insulin-induced gene 1 (Insig-1) and Insig-2 are endoplasmic reticulum membrane–embedded sterol sensors that regulate the cellular accumulation of sterols. Despite their physiological importance, the structural information on Insigs remains limited. Here we report the high-resolution structures of MvINS, an Insig homolog from *Mycobacterium vanbaalenii*. MvINS exists as a homotrimer. Each protomer comprises six transmembrane segments (TMs), with TM3 and TM4 contributing to homotrimerization. The six TMs enclose a V-shaped cavity that can accommodate a diacylglycerol molecule. A homology-based structural model of human Insig-2, together with biochemical characterizations, suggest that the central cavity of Insig-2 accommodates 25-hydroxycholesterol, whereas TM3 and TM4 engage in Scap binding. These analyses provide an important framework for further functional and mechanistic understanding of Insig proteins and the sterol regulatory element–binding protein pathway.

Cholesterol homeostasis is essential for human physiology. Aberrant accumulation of sterols contributes to the initiation and progression of atherosclerosis that can lead to heart attack and stroke (*1*). Cellular sterol levels are monitored by several membrane-embedded proteins, including insulin-induced gene 1 (Insig-1) and Insig-2, which are essential components of the sterol regulatory element–binding protein (SREBP) pathway that controls cellular lipid homeostasis through a feedback inhibition mechanism (*2*–*5*).

SREBPs are a family of membrane-anchored transcription factors that activate genes encoding low-density lipoprotein receptor and enzymes for sterol synthesis (*6*–*8*). SREBP forms a stable complex with SREBP cleavage-activating protein (Scap) through their respective C domains (*9*–*13*). The complex is anchored on the endoplasmic reticulum (ER) through interactions between the membranous domain of Scap and Insig-1/-2 in a sterol-dependent manner (*14*, *15*). Upon cholesterol deprivation, Scap dissociates from Insig-1/-2 and associates with COPII, which translocates the SREBP-Scap complex from the ER to the Golgi (*16*, *17*). In the lumen of the Golgi, SREBP is cleaved by the membrane-anchored site-1 protease (S1P) and then by the intramembrane site-2 protease (S2P) (*18*, *19*), allowing its soluble N-terminal transcription factor domain to enter the nucleus for gene activation (*20*–*23*).

Insig-1/-2 negatively regulate the cellular accumulation of sterols, mainly through two distinct mechanisms. First, upon binding to 25-hydroxycholesterol (25HC), Insig-1/-2 inhibit the exit of the SREBP-Scap complex from the ER, hence preventing transcriptional activation of genes for cholesterol synthesis and uptake (*24*). Second, during sterol repletion, Insig-1 recruits the protein degradation machinery to quickly

[1]State Key Laboratory of Membrane Biology, Tsinghua University, Beijing 100084, China. [2]Center for Structural Biology, School of Life Sciences, School of Medicine, Tsinghua University, Beijing 100084, China. [3]Tsinghua-Peking Center for Life Sciences, Tsinghua University, Beijing 100084, China. [4]National Institute of Biological Sciences, Beijing 102206, China. [5]Molecular Design and Chemical Biology, Therapeutic Modalities, Roche Pharma Research and Early Development, Roche Innovation Center Shanghai, Shanghai 201203, China. [6]Department of Molecular Genetics, University of Texas Southwestern Medical Center, Dallas, TX 75390-9046, USA.
*These authors contributed equally to this work. **†Corresponding author. E-mail: nyan@tsinghua.edu.cn**

Science

Single-trial spike trains in parietal cortex reveal discrete steps during decision-making

Kenneth W. Latimer, Jacob L. Yates, Miriam L. R. Meister, Alexander C. Huk and Jonathan W. Pillow

Science **349** (6244), 184-187.
DOI: 10.1126/science.aaa4056

A better way to explain neuronal activity

A brain region called the lateral intraparietal (LIP) area is involved in primate decision-making. The dominant model to explain neuronal firing in LIP assumes that neurons slowly accumulate sensory evidence in favor of one choice or another. Latimer *et al.* hypothesized that neurons instead exhibit rapid steps or jumps in their firing rate, reflecting discrete changes in the animal's decision state. They recorded from LIP neurons in macaque monkeys performing a motion-discrimination task. LIP spike trains in most cells involved discrete stepping dynamics rather than slow evidence integration dynamics.

Science, this issue p. 184